PCCP

RSC Publishing

PAPER

View Article Online
View Journal | View Issue

Cite this: *Phys. Chem. Chem. Phys.*, 2013, **15**, 5186

Adsorption, dissociation, penetration, and diffusion of N_2 on and in bcc Fe: first-principles calculations

Sang Chul Yeo,[a] Sang Soo Han[b] and Hyuck Mo Lee*[a]

Received 5th December 2012,
Accepted 7th February 2013

DOI: 10.1039/c3cp44367a

www.rsc.org/pccp

We report first-principles calculations of adsorption, dissociation, penetration, and diffusion for the complete nitridation mechanism of nitrogen molecules on a pure Fe surface (bcc, ferrite phase). The mechanism of the definite reaction path was calculated by dividing the process into four steps. We investigated various reaction paths for each step including the energy barrier based on the climb image nudged elastic band (CI-NEB) method, and the complete reaction pathway was computed as the minimum energy path (MEP). The adsorption characteristics of nitrogen (N) and molecular nitrogen (N_2) indicate that nitrogen atoms and molecules are energetically favorable at the hollow sites on pure Fe(100) and (110). The dissociation of the nitrogen molecule (N_2) was theoretically supported by electronic structure calculations. The penetration of nitrogen from the surface to the sub-surface has a large energy barrier compared with the other steps. The activation energy calculated for nitrogen diffusion in pure bcc Fe was in good agreement with the experimental results. Finally, we confirmed the rate-determining step for the full nitridation reaction pathway. This study provides fundamental insight into the nitridation mechanism for nitrogen molecules in pure bcc Fe.

1. Introduction

Nitridation is a typical surface treatment that can enhance the mechanical properties and performance of surfaces with respect to wear, fatigue, and corrosion by incorporating chemically stable nitride compounds.[1–6] Note here that contrary to nitridation, nitration is a process for introducing the nitro (NO_2^-) group. To form a nitride compound, nitrogen should be diffused into pure bcc Fe. To improve the nitridation rate, we must understand the exact reaction mechanism and consider the rate-determining step, which has the highest energy barrier. In addition, the adsorption and dissociation of N_2 molecules represent an area of interest for iron-based catalysts.[7–11] Generally, the rate-determining step in the synthesis of ammonia on iron catalysts is the dissociation of molecular nitrogen.[12,13] Therefore, theoretical and experimental studies on the behavior of nitrogen on Fe surfaces have been conducted by various research groups.

Using Auger electron spectroscopy and low-energy electron diffraction (LEED), Ertl and co-workers found that the adsorption of nitrogen molecules forms a c(2×2) structure on Fe(100) and Fe(111) surfaces.[14–16] They also reported that the adsorption of nitrogen onto potassium promotes the formation of Fe(111) and (100) surfaces.[17] Domain *et al.* reported the results of a theoretical study on the effects of carbon and nitrogen atoms in ferrite (body-centred cubic (bcc) Fe).[18] The Norskov group calculated the interaction of nitrogen with Fe surfaces and the dissociation of N_2 on strained Fe surfaces.[19–21] Their results indicate that the lower barrier for N_2 dissociation is often accompanied by strong nitrogen bonding, which results in the well-known volcano plots of the activity *versus* the d-band filling. Jiang and Carter examined carbon atom adsorption onto, as well as penetration and diffusion into, Fe(100) and Fe(110) surfaces.[22] The energy barriers to diffusion into the Fe(100) and Fe(110) surfaces are 1.18 eV and 1.47 eV, respectively. In addition, the catalytic properties of CO, H_2, O_2, and H_2S on Fe surfaces have been estimated.[23–26] The calculated nitrogen activation energy of 0.8 eV in bcc Fe is in good agreement with experimental findings.[27] Although there are many reports of the behavior of nitrogen on Fe surfaces, the specific nitridation mechanism of N_2 on bcc Fe has not yet been reported, theoretically.

In this study, we divided the complete nitridation mechanism into four steps (adsorption, dissociation, penetration, and diffusion), in which the nitrogen formed various nitride compounds in the iron. Our objective was to determine full reaction pathways for each step, with first principles calculations. First, we investigated the adsorption and dissociation of nitrogen molecules (N_2).

[a] *Department of Materials Science and Engineering, KAIST, 291 Daehak-ro, Yuseong-gu, Daejeon, 305-701, Republic of Korea. E-mail: hmlee@kaist.ac.kr; Fax: +82-42-350-3310; Tel: +82-42-350-3334*

[b] *Center for Nano-characterization, Korea Research Institute of Standards and Science (KRISS), 267 Gajeong-Ro, Yuseong-Gu, Daejeon 305-340, Republic of Korea*

In particular, we analysed the energetic or electronic structure of the Fe surface throughout the nitridation. Next, the dissociative adsorption of nitrogen onto the Fe surface with subsequent diffusion into the interstitial sites (octahedral site) in the sub-surface layer was investigated, which was designated as the second step. In the final step, the penetrating nitrogen diffused into the pure bcc Fe bulk. These steps constitute the complete nitridation mechanism. Finally, a comparison was made at each reaction step to compute the total minimum energy pathway (MEP). The principal factor involved in the overall reaction, which corresponds to the rate-determining step, was determined. The study is organized as follows: in Section 2, we present the computational methods and the system. In Section 3, we provide the calculations for each reaction step for analysing the energy and electronic structures within the MEP. We discuss our findings regarding the rate-determining step in the nitridation process and state our conclusions in Section 4.

2. Computational details

We performed spin-polarized density functional theory (DFT) calculations.[28,29] Code from the Vienna *ab initio* simulation package (VASP) was used to solve the Kohn–Sham equation.[30–32] The VASP is a plane-wave code that uses a projected augmented wave (PAW)[33] and the GGA exchange-correlation functional PBE for structural analyses.[34,35] The energy cut-off for plane waves was 400 eV. The systems and calculation details corresponding to the case in which the Fe(100) and Fe(110) surfaces have more stable surface energies were predominantly used. The surfaces were modelled as periodically repeating (3 × 3) slabs with five layers (the bottom two of which were fixed) and a vacuum of 14 Å on each side (Fig. 1(a) and (b)). For the two-dimensional Brillouin zone,[36] a 5 × 5 × 1 Monkhorst–Pack mesh was used. To accelerate the *k*-point convergence, a Methfessel–Paxton smearing method with a width of 0.2 eV was used. Using the CI-NEB method,[37] each intermediate image is calculated, and an interpolated chain of configurations (images) between the initial and final positions is connected by springs that are simultaneously relaxed. With the appropriate projections, the true force and the spring force acting on each image can be separated from the total force.

The results are refined using a conjugate-gradient minimisation algorithm, and the atomic charge distribution can be analysed *via* Bader charge analysis. In this calculation, we applied a lattice parameter of 2.835 Å, a bulk modulus of 1.76 Mbar, a cohesive energy of 5.16 eV, and a magnetic moment of 2.21 μ_b, which constituted the bulk properties of the pure bcc Fe. The calculated bond length of a N_2 molecule in the gas phase was 1.12 Å, which is in good agreement with the literature.[38] Because the triple N≡N bond has a large binding energy, direct dissociation of a N_2 molecule would be difficult.

The adsorption energies (E_{ad}) of nitrogen were calculated using eqn (1):

$$E_{ad} = E(Fe_{slab}N_m) - E(Fe_{slab}) - \frac{1}{2}E(N_2(g)) \qquad (1)$$

where E (Fe_{slab}) is the total energy of the Fe surface in this system. If a nitrogen atom is used in the calculation, the value of m is 1. However, if a nitrogen molecule is used in the calculation, m equals 2.

3. Results and discussion

A. Adsorption and dissociation of (N, N_2)

We first investigated how a nitrogen atom binds to an Fe surface. The interaction of a N atom on an Fe surface was studied using DFT prior to our investigation of the behavior of the nitrogen molecules (N_2). Each Fe(100) and Fe(110) surface had a specific interaction at its top, bridge, and hollow sites. As shown in Fig. 2, the adsorption properties indicate that all sites with a nitrogen molecule (N_2) prefer hollow sites on Fe(100) and Fe(110), which are the ground state configurations of an adsorbed nitrogen atom on an Fe surface. The adsorption energy (E_{ad}) of Fe(100)/N is −1.66 eV, while that on the Fe(110) surface is

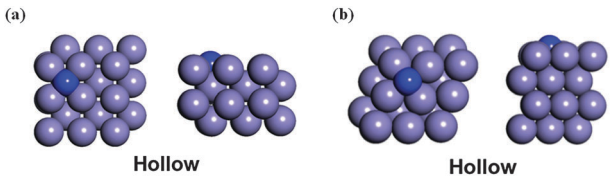

Fig. 2 Ground-state configuration of nitrogen adsorbed onto (a) Fe(100) and (b) Fe(110).

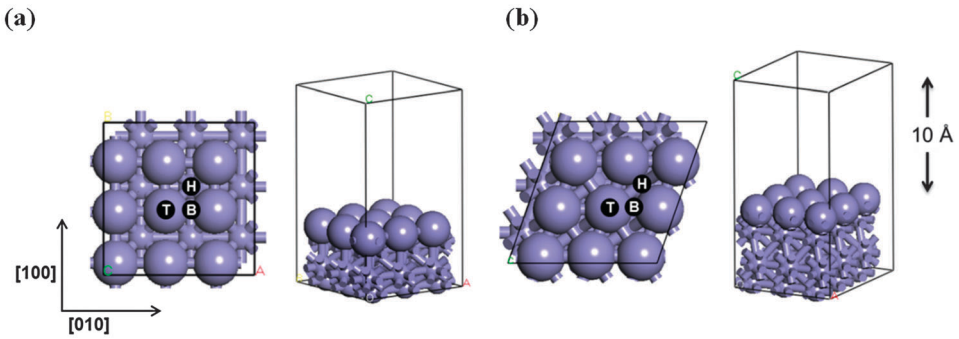

Fig. 1 Schematic top and side views of the (a) Fe(100) and (b) Fe(110) sites: T (top), B (bridge), H (hollow), and a vacuum of 10 Å.

Table 1 The adsorption energy (E_{ad}) of nitrogen for varying coverages (ML) on Fe(100) and Fe(110)

			E_{ad} (eV)			
Configuration	Adsorption site		0 ML	0.22 ML	0.56 ML	1.0 ML
Fe(100)	Top	Hollow	−1.66	−1.35	−1.12	−0.98
	Bridge					
	Hollow					
Fe(110)	Top	Hollow	−1.38	−1.10	−0.97	−0.71
	Bridge					
	Hollow					

−1.38 eV. This difference occurs because the Fe(100) surface has more four-fold symmetric sites than the Fe(110). In a study by Imbihl *et al.* using LEED, N atoms were experimentally found to occupy four-fold hollow sites in a plane that was 0.27 Å above the Fe surface. Mortensen *et al.* examined the adsorption of nitrogen onto Fe(100), Fe(110), and Fe(111) surfaces using a PW91 functional based on GGA-level DFT calculations.[21] They found large binding energy of the N/Fe(100) in the calculation and was also compatible with the high desorption temperature found experimentally.

Next, we demonstrated how the adsorption energy (E_{ad}) changes with increasing nitrogen atom coverage. In Table 1, the adsorption energies (E_{ad}) of the nitrogen on Fe(100) and Fe(110) are shown for varying nitrogen coverages (θ = 0 ML, 0.22 ML, 0.56 ML, 1.00 ML). As the nitrogen coverage increases, the adsorption energy (E_{ad}) decreases. The adsorption energy showed a strong dependence on the coverage, which can be explained by a simple d-band model that the d-band is broadened and lowered in energy by its interaction with the adsorbed nitrogen atoms. Furthermore, we calculated the Fe 4d-band centre for varying nitrogen surface coverages (θ = 0 ML, 0.22 ML, 0.56 ML, 1.00 ML). The d-band centre of the surface Fe atom lowers for a given nitrogen surface coverage (θ = 0 ML, 0.22 ML, 0.56 ML, 1.00 ML), and the d-band was broadened as coverage increases. These results indicate that the surface valence states move down. A comparison of the adsorption energies of nitrogen on Fe(100) and Fe(110) also revealed that the nitrogen binds more strongly to Fe(100) than to Fe(110) for all of the coverages.

The adsorption of nitrogen molecules (N_2) onto Fe surfaces occurs in the gas phase. Thus, to study the nitridation mechanism, we examined the adsorption and dissociation of N_2 molecules in detail. First, we calculated the adsorption energy (E_{ad}) of various sites. Fig. 3 shows the initial configuration of nine adsorption sites divided into six horizontal sites and three vertical sites. We confirmed the bond length after adsorption of the N_2 molecule onto the Fe surface, and the nitrogen molecules were found to have strong adsorption energies on the hollow sites in both their horizontal and vertical configurations. Thus, the adsorption energy (E_{ad}) was high. Because the N_2 molecule has a triple bond with a bond length of 1.12 Å, self-dissociation is difficult. However, once the N_2 molecule was adsorbed onto the Fe surface, the coupling scheme changed as the bond length increased. Thus, the bond strength should have weakened. According to our DFT results shown in Table 2, the nitrogen molecule was strongly adsorbed at the horizontal hollow site 2 on the Fe(100) and Fe(110). The N–N distance was also relaxed by 1.12 Å to 1.28 Å on the Fe(100) surface and 1.26 Å on the Fe(110) surface. In this study, we expected the nitrogen molecule (N_2) to adsorb and subsequently undergo dissociation. Therefore, we used the CI-NEB to obtain the MEP for the nitrogen dissociation reaction. The initial and final configurations could be determined at the lowest energy barrier from the various calculated reaction pathways.

Fig. 4 shows the converged MEP, including the transition state of the nitrogen dissociation on Fe(100) and Fe(110). The two surface types had a final configuration that was lower in energy than the initial configuration, thereby enabling the reaction to easily proceed both thermodynamically and kinetically. The energy difference was exothermic at approximately 1.96 eV on the Fe(100). However, the Fe(110) accounted for 1.27 eV of the energy gap. For the dissociation of a nitrogen molecule (N_2), we obtained

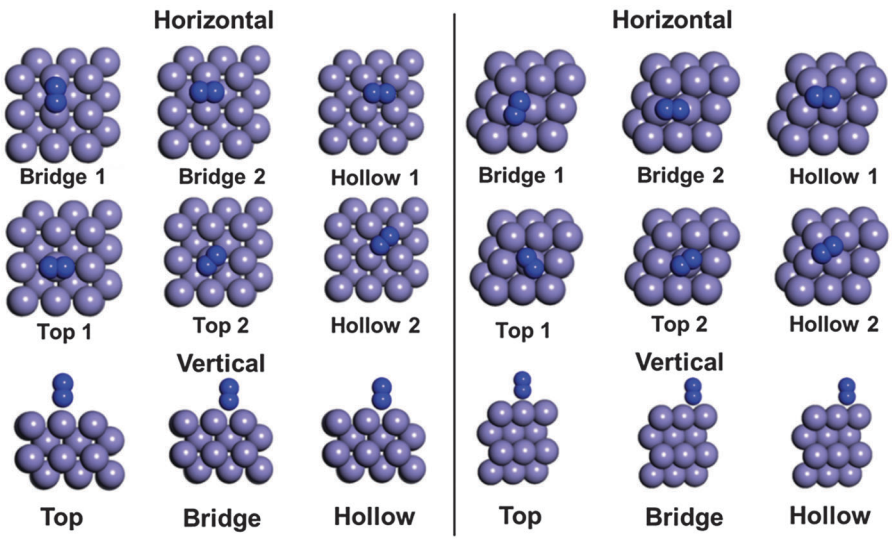

Fig. 3 Sites of the horizontal and vertical adsorption of nitrogen molecules onto Fe(100) and Fe(110).

Table 2 The adsorption energy of molecular nitrogen (N_2) at nine sites on the surfaces of Fe(100) and Fe(110) and the nitrogen-to-nitrogen distance upon adsorption

Sites			E_{ad} (eV)	N–N distance (Å)
Fe(100)	Horizontal	Top 1	−0.096	1.15
		Top 2	−0.092	1.17
		Bridge 1	−0.545	1.19
		Bridge 2	−0.511	1.20
		Hollow 1	−0.965	1.27
		Hollow 2	*−0.977*	*1.28*
	Vertical	Top	−0.546	1.14
		Bridge	−0.516	1.15
		Hollow	−0.935	1.26
Fe(110)	Horizontal	Top 1	−0.055	1.15
		Top 2	−0.012	1.17
		Bridge 1	−0.355	1.16
		Bridge 2	−0.696	1.18
		Hollow 1	−0.946	1.25
		Hollow 2	*−0.955*	*1.26*
	Vertical	Top	−0.620	1.14
		Bridge	−0.574	1.15
		Hollow	−0.921	1.24

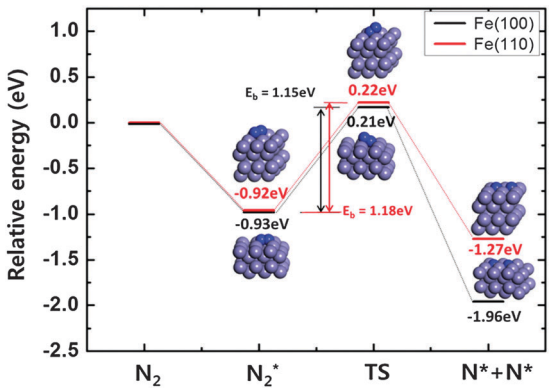

Fig. 4 Minimum energy path (MEP) for the dissociation of nitrogen molecules (N_2) on Fe(100) and Fe(110). The black line represents the reaction on Fe(100), and the red line indicates the reaction on Fe(110).

an energy barrier of 1.15 eV on Fe(100) and 1.18 eV on Fe(110). Energetically, the total energy of the dissociated nitrogen (2N) on the Fe(100) is more stable than that on the Fe(110), although energy barriers for the N_2 dissociation are similar on Fe(100) and Fe(110), which indicates that the dissociation of N_2 on Fe(100) is thermodynamically more favorable than on Fe(110).

Bozso *et al.* reported that the activation energies for nitrogen dissociation on Fe(100) and Fe(110) are 21 and 27 kJ mol^{-1}, respectively.[39,40] Egeberg *et al.* and other groups have noted that DFT calculations predict a substantially higher activation barrier for N_2 dissociation on a clean Fe(110) surface compared to a strained Fe/Ru (0001) surface.[41] However, the experimental activation barriers were substantially lower than predicted for both surfaces. In this study, Fig. 4 shows the MEP for the dissociation of nitrogen. In the complete energy pathway, Fig. 4 corresponds to the initial state, the transition state, and the final state, respectively. In the transition state, we examined the configuration of the N_2 molecule. One of the two nitrogen atoms was localised at the hollow site with a relaxed bonding length. The nitrogen transferred an electron to the neighbouring Fe atoms. The electronic structure was analysed in detail using both charge transfer and orbital analysis.

B. Electronic structure analysis

Next, we sought to investigate why the dissociation of N_2 molecules on the Fe surface had a lower energy barrier than the binding of N_2 (−9.73 eV) to this surface. We examined how the charge transfer was affected by the interaction between the nitrogen and the Fe surface. Table 3 shows the average Bader charge and bond length for nitrogen in the initial state, adsorption state, transition state (TS), and dissociation state.

In general, nitrogen has seven electrons with bonding orbitals occupied up to the σ_{2px} molecular orbital; the highest occupied molecular orbital (HOMO) is the σ_{2px} molecular orbital, and the lowest unoccupied molecular orbital (LUMO) is the π_{2py}^* molecular orbital. Because the π_{2py}^* molecular orbital is an anti-bonding level, we predicted that the bonding strength of the nitrogen molecule (N_2) would weaken if the nitrogen received an electron in the p-state when bonding to the Fe surface. Therefore, we analysed the electron transfer in the p-state and examined the average Bader charge of each state.[42,43] In the adsorption stage, the average Bader charge was transferred with $-0.4995e$, and the interatomic distance of nitrogen was 1.2803 Å. We assumed that the nitrogen bonded as a free nitrogen molecule. Next, we calculated the relaxed bond lengths from the transition state to the dissociation state. Finally, the dissociated nitrogen atoms were stabilized at the hollow site. Additionally, the average Bader charge became increasingly negative as the electrons were accepted, as shown in Fig. 5. Consequently, after the adsorption of N_2 onto the hollow site on the Fe surface, the Fe atoms could easily donate electrons in the Fe d-state to the N_2. The electron, which was occupied in the anti-bonding state (π_{2py}^*), reduced the bond strength of the N_2.

Based on its magnetic moment, Logadottir *et al.*[41] reported that the bcc Fe surface is ferromagnetic and that the magnetic moment for the surface is 2.51/atom μ_b/atom, which does not greatly differ from the value of bulk bcc Fe (2.20/atom μ_b/atom) obtained by the DFT calculation. In addition, S. J. Jenkins calculated magnetic moment enhancements in the surface layer (due to a narrowing of the d-band leading to a large

Table 3 The average Bader charge and the bond length of nitrogen molecules on Fe(100) and Fe(110). A negative charge value indicates that the electrons are transferred from the surface to the adsorbates, whereas a positive value indicates the opposite

	Initial	Adsorption	Transition state	Dissociation
Fe(100)				
q (N_2) [e per molecule]	—	−0.4995	−0.5006	−0.49445
Bond length [Å]	1.117	1.2803	1.8489	2.958
Fe(110)				
(N_2) [e per molecule]	—	−0.4567	−0.2511	−0.4093
Bond length [Å]	1.117	1.2572	1.7618	2.8839

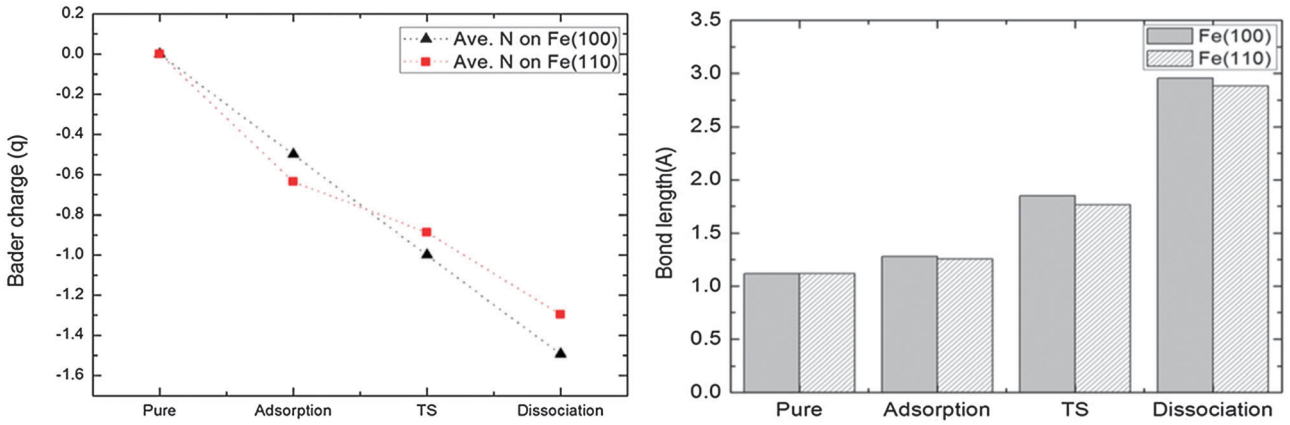

Fig. 5 The average Bader charge and bond length of nitrogen at each state. The black line indicates the Bader charge analysis on Fe(100). The red line denotes the Bader charge analysis on Fe(110). The filled box shows the bond length of Fe(100), and the checked box shows the bond length of Fe(110) at each configuration.

Stoner parameter) for a wide variety of 3d ferromagnetic surfaces.[11] Interestingly, the adsorption of molecular species at ferromagnetic surfaces has been found to cause a marked reduction in the surface magnetic moments. They demonstrated that the effect was strongly localized on the surface atoms directly involved in the adsorbate–substrate covalent bonding. The adsorbate was found to gain a net minority spin polarisation. This antiferromagnetic coupling could be explained by the synergic charge flow, which is in good agreement with the results for the average Bader charge.

C. Penetration and diffusion of the nitrogen atom

We performed a DFT calculation to determine the MEP for the penetration of nitrogen atoms from the surface to the subsurface based on the CI-NEB method, and the results are shown in three images. Fig. 6 shows the optimal energy pathway for the nitrogen penetration. The energy barrier for the nitrogen penetration has a high energy barrier. As a result, Fe(100) has a higher energy barrier (1.82 eV) than Fe(110) (1.97 eV). In addition, Fe(110) requires more endothermic energy than Fe(100). These results demonstrate the presence of a higher energy barrier in comparison to the dissociation energy barrier for a nitrogen molecule (N_2). The E. A. Carter group demonstrated that a carbon atom diffuses into Fe(100) and Fe(110) with energy barriers of 1.18 and 1.47 eV, respectively.[22] Our results indicate that Fe(100) has a lower energy barrier than Fe(110). According to these results, Fe(100) is the favored surface for an N penetration reaction.

Considering simple, first-order, Arrhenius-type diffusion [$\nu = \nu_0 \exp(-E/k_bT)$],[47,48] the temperature (T) for an N-hopping

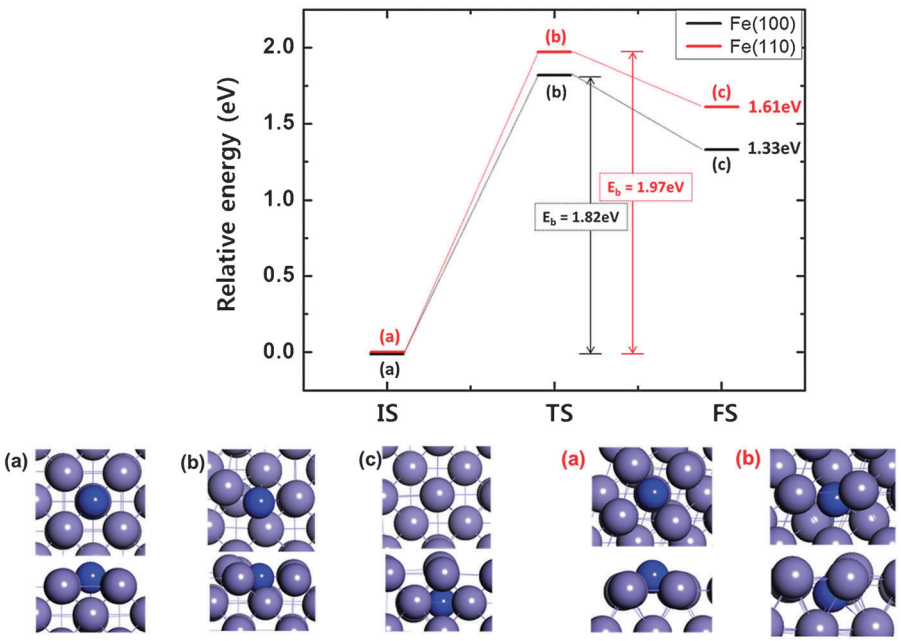

Fig. 6 The minimum energy path (MEP) for the penetration of dissociated nitrogen into Fe(100) and Fe(110): (a) initial state, (b) transition state, and (c) final state. The black line represents the reaction on Fe(100); the red line indicates the reaction on Fe(110).

event (ν) can be approximately calculated if we use an attempt frequency ν_0 equivalent to the Debye frequency of 10^{13} Hz, an energy barrier E of 1.82 eV for Fe(100) and 1.97 eV for Fe(110), and a hop rate of 1 hop per second, which is consistent with experimentally observed nitridation rates, to yield temperatures of 665 and 774 K, which are in good agreement with the experimental nitridation process temperature.[44–46]

To investigate nitrogen diffusion in pure bcc Fe, we constructed an energy diagram for the diffusion of nitrogen in bcc iron. The behavior of nitrogen atoms in interstitial diffusion is generally well known. In a previous study, we reported that nitrogen is stable in octahedral interstitial sites. If the activation energy of nitrogen is confirmed in pure bcc-Fe, we can calculate a diffusion coefficient. To obtain the energy barrier for nitrogen, we utilized the CI-NEB method. Our result (0.73 eV) is in good agreement with the experimental results,[47,48] as shown in Fig. 7. Jiang and Carter reported that the diffusion of carbon in bcc iron has a barrier of 0.86 eV, which is in excellent agreement with the experimental value of 0.87 eV, suggesting an MEP of carbon diffusion from an octahedral site to another octahedral site *via* a tetrahedral site, which constitutes a transition state.[38]

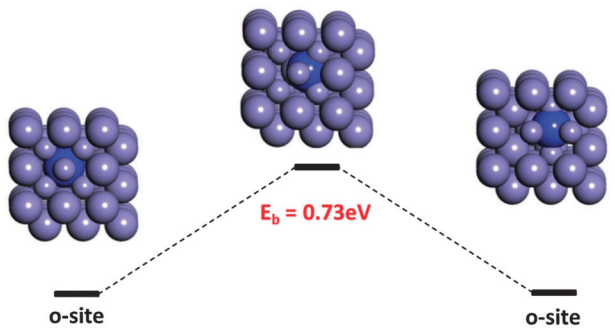

Fig. 7 Energy diagram of the activation energy for nitrogen diffusion in bcc Fe from one octahedral site (o-site) to another octahedral site (o-site).

D. Total nitridation reaction pathway of a nitrogen molecule (N_2)

A schematic diagram for the total MEP of the nitridation mechanism is shown in Fig. 8. We described four steps along the complete reaction pathway. Additionally, we found a slight difference in the MEPs for the nitridation reactions with Fe(100) and Fe(110). According to the total energy diagram, Fe(100) is a favorable surface for N_2 adsorption, dissociation, and penetration. At each step, a transition state existed, and it was possible to compare the energy barriers between each state (E_b). Overall, the rate-determining step for nitridation was determined to be the penetration step because it had the highest energy barrier of the four steps.

4. Conclusion

In summary, we performed first-principles calculations to observe the full nitridation mechanism of a nitrogen molecule (N_2) in bcc Fe (ferrite). This mechanism is typically divided into four steps: adsorption, dissociation, penetration, and diffusion. First, the adsorption mechanisms of nitrogen atoms and nitrogen molecules (N_2) were determined. Then, the dissociation of nitrogen molecules (N_2) was calculated according to the MEP based on the CI-NEB method. The N–N bond length (N_2) was easily relaxed at the strongest adsorption site (the hollow site). In addition, the dissociation energy barrier was lower than predicted. With regard to the electronic structure, nitrogen molecules have a unique property in their electronic structure whereby electrons are transferred from the neighboring Fe atoms. Thus, we analysed the p-state spin, the average Bader charge, the highest occupied molecular orbital (HOMO), and the lowest unoccupied molecular orbital (LUMO) and compared the bond lengths. The trends on the adsorption of N_2 onto the hollow site on the Fe surface, the Fe atoms could easily donate electrons in the Fe d-state to the N_2. The electron, which

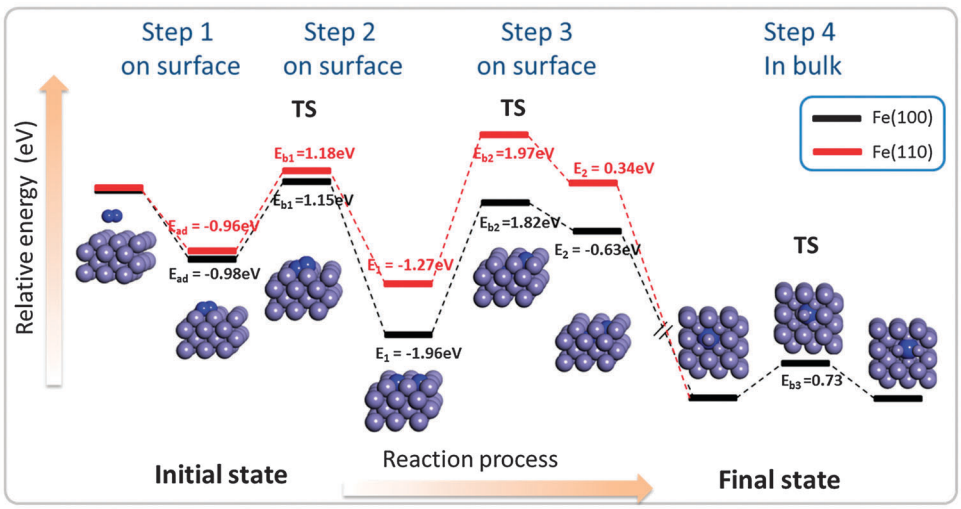

Fig. 8 Energy diagram of molecular nitrogen (N_2) in bcc Fe. The black line indicates its behavior in Fe(100), and the red line shows its behavior in Fe(110).

was occupied in the anti-bonding state, reduced the bond strength of the N_2. The penetration step was found to have a higher energy barrier than the other steps. Using the CI-NEB method, an activation energy of 0.73 eV was calculated for the diffusion of nitrogen in pure bcc Fe. Finally, we completed our analysis of the full nitridation mechanism for nitrogen molecules by determining the MEP. We identified the steps that determine the nitridation rate and found that the rate-determining step was step 3 (penetration of the nitrogen). Furthermore, we suggested a creative method by which nitridation of the surface layer can be controlled through the substitution of impurities with N atoms at the surface layer, thereby enabling an enhancement of the nitridation rate.

Acknowledgements

We appreciate helpful discussions with Prof. Ju Li from Department of Nuclear Science and Engineering and Department of Materials Science and Engineering, Massachusetts Institute of Technology, Cambridge, Massachusetts, USA. This work was financially supported by the POSCO and Advanced Technology Center project 2011-10031476, and a National Research Foundation of Korea (NRF) grant funded by the Korean government (MEST) (2011-0028612).

References

1 T. Weber, L. Dewit, F. W. Saris, A. Koniger, B. Rauschenbach, G. K. Wolf and S. Krauss, *Mater. Sci. Eng., A*, 1995, **199**, 205–210.
2 D. K. Inia, M. H. Propper, W. M. Arnoldbik, A. M. Vredenberg and D. O. Boerma, *Appl. Phys. Lett.*, 1997, **70**, 1245–1247.
3 S. A. Gerasimov, A. V. Zhikharev, V. A. Golikov and Y. Y. Lavrova, *Met. Sci. Heat Treat.*, 2001, **43**, 462–463.
4 X. Luo and S. X. Liu, *J. Magn. Magn. Mater.*, 2007, **308**, L1–L4.
5 L. Nosei, S. Farina, M. Avalos, L. Nachez, B. J. Gomez and J. Feugeas, *Thin Solid Films*, 2008, **516**, 1044–1050.
6 W. P. Tong, N. R. Tao, Z. B. Wang, J. Lu and K. Lu, *Science*, 2003, **299**, 686–688.
7 Z. Kowalczyk, J. Sentek, S. Jodzis, M. Muhler and O. Hinrichsen, *J. Catal.*, 1997, **169**, 407–414.
8 B. Fastrup, *J. Catal.*, 1994, **150**, 345–355.
9 M. Muhler, F. Rosowski and G. Ertl, *Catal. Lett.*, 1994, **24**, 317–331.
10 J. Zielinski, L. Znak and Z. Kowalczyk, *Langmuir*, 2002, **18**, 10191–10195.
11 S. J. Jenkins, *Surf. Sci.*, 2006, **600**, 1431–1438.
12 A. Jedynak, Z. Kowalczyk, D. Szmigiel, W. Rarog and J. Zielinski, *Appl. Catal., A*, 2002, **237**, 223–226.
13 A. Jedynak, D. Szmigiel, W. Rarog, J. Zielinski, J. Pielaszek, P. Dluzewski and Z. Kowalczyk, *Catal. Lett.*, 2002, **81**, 213–218.
14 R. Imbihl, R. J. Behm, G. Ertl and W. Moritz, *Surf. Sci.*, 1982, **123**, 129–140.
15 G. Ertl, S. B. Lee and M. Weiss, *Surf. Sci.*, 1982, **114**, 515–526.
16 G. Ertl, M. Grunze and M. Weiss, *J. Vac. Sci. Technol.*, 1976, **13**, 314–317.
17 G. Ertl, S. B. Lee and M. Weiss, *Surf. Sci.*, 1982, **114**, 527–545.
18 C. Domain, C. S. Becquart and J. Foct, *Phys. Rev. B: Condens. Matter Mater. Phys.*, 2004, **69**, 144112.
19 R. C. Egeberg, S. Dahl, A. Logadottir, J. H. Larsen, J. K. Norskov and I. Chorkendorff, *Surf. Sci.*, 2001, **491**, 183–194.
20 J. J. Mortensen, L. B. Hansen, B. Hammer and J. K. Norskov, *J. Catal.*, 1999, **182**, 479–488.
21 J. J. Mortensen, M. V. Ganduglia-Pirovano, L. B. Hansen, B. Hammer, P. Stoltze and J. K. Norskov, *Surf. Sci.*, 1999, **422**, 8–16.
22 D. E. Jiang and E. A. Carter, *Phys. Rev. B: Condens. Matter Mater. Phys.*, 2005, **71**, 045402.
23 D. E. Jiang and E. A. Carter, *J. Phys. Chem. B*, 2004, **108**, 19140–19145.
24 D. E. Jiang and E. A. Carter, *Surf. Sci.*, 2005, **583**, 60–68.
25 D. E. Jiang and E. A. Carter, *Surf. Sci.*, 2003, **547**, 85–98.
26 D. E. Jiang and E. A. Carter, *Surf. Sci.*, 2004, **570**, 167–177.
27 A. D. L. Claire, in *Numerical Data and Functional Relationships in Science and Technology*, 1990, vol. 26, ch. 8, pp. 480–481.
28 E. J. Baerends, *Theor. Chem. Acc.*, 2000, **103**, 265–269.
29 M. Ernzerhof and G. E. Scuseria, *Theor. Chem. Acc.*, 2000, **103**, 259–262.
30 G. Kresse and J. Furthmuller, *Comput. Mater. Sci.*, 1996, **6**, 15–50.
31 G. Kresse and D. Joubert, *Phys. Rev. B: Condens. Matter Mater. Phys.*, 1999, **59**, 1758–1775.
32 G. Kresse and J. Furthmuller, *Phys. Rev. B: Condens. Matter Mater. Phys.*, 1996, **54**, 11169–11186.
33 P. E. Blochl, *Phys. Rev. B: Condens. Matter Mater. Phys.*, 1994, **50**, 17953–17979.
34 J. P. Perdew, K. Burke and M. Ernzerhof, *Phys. Rev. Lett.*, 1996, **77**, 3865–3868.
35 J. P. Perdew, K. Burke and M. Ernzerhof, *Phys. Rev. Lett.*, 1997, **78**, 1396.
36 M. Methfessel and A. T. Paxton, *Phys. Rev. B: Condens. Matter Mater. Phys.*, 1989, **40**, 3616–3621.
37 G. Henkelman, B. P. Uberuaga and H. Jonsson, *J. Chem. Phys.*, 2000, **113**, 9901–9904.
38 D. E. Jiang and E. A. Carter, *Phys. Rev. B: Condens. Matter Mater. Phys.*, 2003, **67**, 214103.
39 F. Bozso, G. Ertl, M. Grunze and M. Weiss, *J. Catal.*, 1977, **49**, 18–41.
40 F. Bozso, G. Ertl and M. Weiss, *J. Catal.*, 1977, **50**, 519–529.
41 A. Logadottir and J. K. Norskov, *Surf. Sci.*, 2001, **489**, 135–143.
42 G. Henkelman, A. Arnaldsson and H. Jonsson, *Comput. Mater. Sci.*, 2006, **36**, 354–360.
43 W. Tang, E. Sanville and G. Henkelman, *J. Phys.: Condens. Matter*, 2009, **21**, 084204.
44 M. A. J. Somers and E. J. Mittemeijer, *Metall. Mater. Trans. A*, 1995, **26**, 57–74.
45 R. E. Schacherl, P. C. J. Graat and E. J. Mittemeijer, *Z. Metallkd.*, 2002, **93**, 468–477.
46 H. Du and J. Agren, *Z. Metallkd.*, 1995, **86**, 522–529.
47 Y. Iijima, *J. Alloys Compd.*, 1996, **234**, 290–294.
48 J. Silva and R. B. McLellan, *Mater. Sci. Eng.*, 1976, **26**, 83–87.

